Computers & Geosciences ▮ (▮▮▮▮) ▮▮▮–▮▮▮

Contents lists available at ScienceDirect

Computers & Geosciences

journal homepage: www.elsevier.com/locate/cageo

On the simulation of continuous in scale universal multifractals, Part II: Space–time processes and finite size corrections

S. Lovejoy [a,b,*], D. Schertzer [c,d]

[a] Department of Physics, McGill University, 3600 University Street, Montreal, Que., Canada
[b] GEOTOP, UQAM, CP 8888, Succ. Centre Ville, Montreal, Que., Canada H3C 3P8
[c] Université Paris-Est, ENPC/CEREVE, 77455, Marne-la-Vallee Cedex 2, France
[d] Météo France, 1 Quai Branly, 75007 Paris, France

ARTICLE INFO

Article history:
Received 23 July 2010
Accepted 23 July 2010

Keywords:
Multifractals
Fractals
Scaling
Turbulence
Numerical simulations

ABSTRACT

In Part I we considered continuous in scale cascade processes which were spatially continuous; these are needed for modeling many geofields. In this second part we consider the effects of spatial discretization; this allows us to make numerical simulations. We show how to correct the simulations for the leading finite size effects, for both space and (causal) space–time processes. The resulting processes have significantly improved small scale statistical properties; in practice it can lead to great savings in computer time and memory usage. In an appendix we give a *Mathematica* code for the corresponding space–time simulations.

1. Introduction

Geofields typically exhibit strong nonlinear variability with structures spanning such huge ranges of space–time scales that classical modeling and statistical approaches which rely on smoothness, regularity or other homogeneity assumptions are often impotent. Scaling approaches predicated on intrinsic wide scale range dynamics therefore provide natural geoscience frameworks. It is thus hardly surprising that, alternative attempts to conceptualize and model geophenomena using scaling ideas already have long histories. In solid earth geophysics, they go back nearly 100 years to when Perrin (1913) eloquently argued that the coast of Brittany was nondifferentiable. Later, Steinhaus (1954) expounded on the nonintegrability (“nonrectifiability”) of the river Vistula, Richardson (1961) quantified both aspects using scaling exponents and Mandelbrot (1967) interpreted the exponents in terms of fractal dimensions. Indeed, scaling in the earth’s surface is so prevalent that there are entire scientific specializations such as river hydrology and geomorphology which abound in scaling laws of all types (see e.g. Rodriguez-Iturbe and Rinaldo (1997)). In atmospheric dynamics, scaling approaches go back to Richardson (1922)’s poetic evocation of cascade processes, and his proposal that the trajectories of air particles resemble (fractal) Wierstrasse functions (Richardson, 1926). All the classical theories of small scale (isotropic 3D) turbulence (Kolmogorov, 1941; Corrsin, 1951; Obukhov, 1949, 1959; Bolgiano, 1959) as well as their large scale (isotropic 2-D) counterparts (Kraichnan, 1967; Charney, 1971) are built around scaling – and indeed cascade – assumptions.

Over the last thirty years there has been great progress in understanding and modeling scaling systems. For example they have been generalized from the restrictive classical isotropic scaling notions associated with self-similar fractals: it has been found that they can respect anisotropic scaling symmetries in which the small and large scales are related by scale changing operations involving not only “zooms” but also squashing and rotation of structures with scale. In addition, it has become increasingly clear that the appropriate framework for scaling mathematical fields (as opposed to scaling geometric sets of points) is multifractals (rather than fractal sets), and that multiplicative cascades are the generic multifractal process. Indeed, the key solid earth field – the topography – has been found to be scaling over huge ranges (see Gagnon et al. (2006) and the review, Lovejoy and Schertzer (2007)) and atmospheric radiances at long and short wavelengths follow very closely the predictions of multiplicative cascade models (see Lovejoy et al. (2009) and the review, Lovejoy and Schertzer (2010)). Today, there is hardly a geoscience in which there have not been claims of multifractal statistics—at least over some range of scales. While it may be true that over finite (usually narrow) ranges of scales, nonfractal processes can always be concocted that approximate the fields, since multifractals are the generic scaling process they nevertheless provide parsimonious initial wide scale range models of

* Corresponding author at: Department of Physics, McGill University, 3600 University Street, Montreal, Que., Canada. Tel.: +1 514 398 6537.
E-mail address: lovejoy@physics.mcgill.ca (S. Lovejoy).

0098-3004/$ - see front matter © 2010 Elsevier Ltd. All rights reserved.
doi:10.1016/j.cageo.2010.07.001

geoprocesses. Recently, this has perhaps been stunningly demonstrated on the most prestigious numerical weather models: Stolle et al. (2009) have shown that these have nearly exactly multiplicative cascade structures (and are hence multifractals) over almost their entire ranges. It is therefore hardly an exaggeration to say that cascades and multifractals are ubiquitous in the geosciences.

Paradoxically, the theoretical and numerical techniques needed to model cascades are still highly underdeveloped; indeed, as pointed out in Part I of this series, rather than having dynamics based on a continuum of scales, they are almost all unrealistically based on integer powers of discrete scale ratios. In Part I, we considered the main exception, the fractionally integrated flux (FIF) process which is a continuous in scale cascade process. By using a pure truncated power law for the weighting function g, we showed how we can obtain the correct (power law) one-point statistics for a multiscaling process ε_λ at resolution λ: $\langle \varepsilon_\lambda^q \rangle = \lambda^{K(q)}$ with $K(q) = (C_1/(\alpha-1))(q^\alpha - q)$ where α is the Levy index and C_1 is the codimension of the mean field. However, when considering such a cascade developed over a fixed range of scales, the internal statistical structure was not perfectly scaling. For example, when we calculated the corresponding two-point correlation function $\langle \varepsilon_\lambda(\underline{x})\varepsilon_\lambda(\underline{x}-\underline{\Delta x})\rangle$ we found that it had extra multiplicative corrections to the pure power law $|\underline{\Delta x}|^{-K(2)}$; the leading one was $e^{(-2\alpha^2/((\alpha-1)D)|\underline{\Delta x}|^{-D/\alpha}}$ and its effect disappeared very slowly, especially for the larger α values. In this second part, we consider processes discrete in space and in space–time necessary for numerical implementations; for simplicity we concentrate on the $D=1$ and 2 dimensional (both casual and acausal) cases while indicating the straightforward generalizations to higher D.

2. One-point statistics

2.1. The spatially discrete generator

Consider a 1-D simulation with a total of λ points with inner scale 1; distribute them between $-\lambda$ and λ using a discretisation over odd integer x; this implies that the grid elements are of intervals of length $\Delta X=2$. With λ points, changing the grid spacing from 2 to 2δ is the same as changing λ to $\lambda\delta$ so that the range of scales is the same, there is no advantage of using finer resolution.

We now repeat the steps indicated in Section 2 Part I for the continuous in scale acausal processes. The generator Γ is now

$$\Gamma_\lambda(\underline{x}) = C_1^{1/\alpha} N_{D,f}^{-1/\alpha} \sum_{-\lambda \le x' \le \lambda, odd} \gamma(x-x') g(x')\, dx' \quad (1)$$

(cf. the continuous Eq. (18), Part I). Note that the discrete normalization constant $N_{D,f}$ is not the same as the continuous N_D, see Eqs. (7) and (8) below. The SCF of Γ are therefore

$$K_\Gamma(q) = \log \langle e^{q\Gamma_\lambda} \rangle = \frac{C_1}{\alpha-1} q^\alpha N_{D,f}^{-1} \sum_{-\lambda \le x' \le \lambda, odd} g(\underline{x}')^\alpha \quad (2)$$

as before, we must choose g such that $\sum g^\alpha \propto \log \lambda$. As discussed in Part I, in causal processes, $g(\underline{x}, t)$ must be zero for $t<0$. A simple way to achieve this is to multiply by a Heaviside function $\theta(t)$ (such that $\theta(t)=1$ $(t \ge 0), =0$, $(t<0)$) so that an acausal $g(\underline{x}, t)$ can be transformed into the causal function: $g_c(\underline{x}, t) = \theta(t)\, g(\underline{x}, t)$. In 1-D (with t in place of $\underline{x}$), this is equivalent to summing in Eq. (2) only over $1 \le x' \le \lambda$.

2.2. The Euler–Machlaurin sum rule

We first consider the one-point statistics; since we already have the results for the spatially continuous process it is convenient to use the Euler–Maclauren formula which for an arbitrary function f relates integrals and sums (the first order formula is the familiar "trapezoidal rule")

$$\sum_{j=0}^{n} f(u+j\Delta X) = \frac{1}{\Delta X}\int_u^v f(x)\, dx + \frac{1}{2}(f(u)+f(v)) + \left(\Delta X \frac{B_2}{2!} f'(x)\Big|_u^v + \Delta X^3 \frac{B_4}{4!} f'''(x)\Big|_u^v + \cdots\right); \quad v = u + n\Delta X \quad (3)$$

with the Bernoulli numbers: $B_2=1/6$, $B_4=-1/30$, $B_6=1/42$.

We see that the difference between the sum and integral involves a series of "boundary" terms. We must use the above formula with $\Delta X=2$ and apply it to $f=g^\alpha$

$$\sum_{-\lambda \le x < \lambda, odd} g(x)^\alpha = \frac{1}{2}\int_{-\lambda}^{-1} g(x)^\alpha\, dx + \frac{1}{2}\int_1^\lambda g(x)^\alpha\, dx + \frac{1}{2}(g(-\lambda)^\alpha + g(-1)^\alpha + g(1)^\alpha + g(\lambda)^\alpha) + \frac{1}{6}\left[-\frac{\partial g(x)^\alpha}{\partial x}\Big|_{x=-\lambda} + \frac{\partial g(x)^\alpha}{\partial x}\Big|_{x=-1} - \frac{\partial g(x)^\alpha}{\partial x}\Big|_{x=1} + \frac{\partial g(x)^\alpha}{\partial x}\Big|_{x=\lambda}\right] - O\left(\frac{\partial^3 g(x)^\alpha}{\partial x^3}\right) \quad (4)$$

We can now apply the formula to the symmetric acausal case

$$\sum_{-\lambda \le x < \lambda, odd} g(x)^\alpha = \int_1^\lambda g(x)^\alpha\, dx + g(1)^\alpha + g(\lambda)^\alpha + \frac{1}{3}\left[\frac{\partial g(x)^\alpha}{\partial x}\Big|_{x=\lambda} - \frac{\partial g(x)^\alpha}{\partial x}\Big|_{x=1}\right] + O\left(\frac{\partial^3 g(x)^\alpha}{\partial x^3}\right) \quad (5)$$

Taking g as a truncated power law (Eq. (20)) Part I we obtain

$$\textstyle\sum_{-\lambda \le x < \lambda, odd} |x|^{-1} = (b + \log \lambda);\ b = \gamma_E + \log 2 + \lambda^{-1} + O(\lambda^{-2}) \quad (6)$$

($\gamma_E=0.577$ … is the Euler number, see Schertzer and Lovejoy, 1987). We see that to obtain the correct leading $\log \lambda$ behaviour the finite difference normalization factor must satisfy

$$N_{D,f} = N_D/\Delta X \quad (7)$$

In D dimensions, the corresponding formula for acausal processes is clearly

$$N_{D,f} = N_D/\Delta X^D \quad (8)$$

In $D=1$, we have $N_{D,f}=2/2=1$. When comparing isotropic acausal processes (with $g(\underline{x}, t)=g(\underline{x}, -t)$) and the corresponding causal processes (with $g_c(\underline{x}, t)=\theta(t)\, g(\underline{x}, t)$), the domain of integration/summing is halved so that the difference is a factor of 2, hence $N_{D,f,c}=N_{D,f}/2$.

To understand the effect of the nonlogarithmic terms, write

$$\varepsilon_{\lambda,f,u}(x) = e^{C_1^{1/\alpha} \sum_{-\lambda \le x' \le \lambda, odd} \gamma(x-x')g(x')} = \varepsilon_{\lambda,u}(x) e^B$$
$$\langle \varepsilon_{\lambda,f,u}^q \rangle = \langle e^{q\Gamma_{\lambda,f}} \rangle = e^{\frac{C_1}{\alpha-1} \sum_{-\lambda \le x' \le \lambda, odd} g(x')^\alpha} = \lambda^{\frac{C_1}{\alpha-1}q^\alpha} e^{\frac{C_1}{\alpha-1}bq^\alpha} \quad (9)$$

(using $N_{D,f}=1$). The first equation is for the random field, the second is for the statistics. We have used the subscript "f" for "finite element" and "u" for "unnormalized"; $\varepsilon_{\lambda,u}$ is the theoretical unnormalized (continuous in space) field discussed in Section 2. In the above, B is random Levy variable corresponding to the b term in Eq. (6)

$$B = C_1^{1/\alpha} b^{1/\alpha} \gamma_\alpha$$

Please cite this article as: Lovejoy, S., Schertzer, D., On the simulation of continuous in scale universal multifractals, Part II: Space–time processes and finite size corrections. Computers and Geosciences (2010), doi:10.1016/j.cageo.2010.07.001

$$\langle e^{qB}\rangle = e^{(C_1/\alpha-1)bq^\alpha} \tag{10}$$

where γ_α is a unit extremal Levy variable index α. We therefore see that the effect of the nonlogarithmic terms is to multiply the process by an exponentiated Levy variable so that the result is too variable (possibly wildly so) depending on C_1, α. Alternatively, defining $\log\lambda' = \log\lambda + b$, we see that the (bare) statistics are those of a process with scale ratio $\lambda' = \lambda e^b$ rather than λ. Using the large λ limiting value $b \approx 1.27$, we find $\lambda'/\lambda = 3.56$.

2.3. Normalization

We must now produce a normalized process from the unnormalized spatially discrete realization $\varepsilon_{\lambda,f,u}$. To understand this, recall that we seek a finite element approximation to the continuous in space normalized process

$$\langle \varepsilon_{\lambda,n}^q\rangle = \lambda^{K(q)}; \quad K(q) = \frac{C_1}{\alpha-1}(q^\alpha - q)$$
$$\varepsilon_{\lambda,n} = \frac{\varepsilon_{\lambda,u}}{\langle \varepsilon_{\lambda,u}\rangle} \tag{11}$$

From this (and Eq. (9)), we see that due to the additional e^B factor that the normalization for the spatially discrete ε is a bit more involved than for the spatially continuous ε; at the level of random variables, we have

$$\varepsilon_{\lambda,f,u} = \varepsilon_{\lambda,n}\langle \varepsilon_{\lambda,u}\rangle e^B \tag{12}$$

The multiplication by the generally widely varying e^B factor suggests that one perform a "microcanonical" normalization, i.e. to separately normalize each realization by its spatial mean

$$\varepsilon_{\lambda,f,n} = \frac{\varepsilon_{\lambda,f,u}}{\overline{\varepsilon_{\lambda,f,u}}}; \quad \overline{\varepsilon_{\lambda,f,u}} = \lambda^{-1}\sum_{i=1}^{\lambda}\varepsilon_{\lambda,f,u}(i) \tag{13}$$

where the sum/dressing is over all the λ values of the simulation; this normalization is the one used in the simulations shown earlier. Comparing this with the definition of the dressed and hidden factors in Part I Section 1.3 combining Eqs. (12) and (13) we find

$$\varepsilon_{\lambda,f,n} = \frac{\varepsilon_{\lambda,n}}{\varepsilon_{\lambda,\lambda(h)}}$$
$$\langle \varepsilon_{\lambda,f,n}^q\rangle = \lambda^{K(q)}\langle \varepsilon_{\lambda,\lambda(h)}^{-q}\rangle \tag{14}$$

i.e. with this easy to perform normalization, we replace the wildly varying e^B factor with the random factor $\varepsilon_{\lambda,\lambda(h)}$which for $q < q_D$, is typically of order unity (Schertzer and Lovejoy, 1987). Since $\langle \varepsilon_{\lambda,\lambda(h)}^{-q}\rangle < 1$ for $q > 1$, the microcanonically normalized simulation is therefore a bit too calm at the largest scales (as found in the simulations, see Part I Fig. 5). In any case, none of these issues affect the internal statistics (such as the autocorrelation) of realizations of the process. For reference, for all α we have $q_D \geq D/C_1$ so that for the simulations here with $D=1$, $C_1=0.2$, $q_D \geq 5$ so that the moments shown in Part I Figs. 5 and 6 are of too low an order to be divergent. A further note on the statistics: even without the divergence of moments there is another source of singular statistics ("multifractal phase transitions", see e.g. Szépfalusy et al. (1987)), which arises when the statistical moments are dominated by a single extreme large value. Schertzer et al. (1993) show that for finite samples with N_s realizations that the effective dimension of the sample is $D+D_s$, $D_s = \log N_s/\log\lambda$. There is then another critical moment $q_s = ((D+D_s)/C_1)^{1/\alpha}$ and if $q_s < q_D$ then only moments $q < q_s$ will be reliably estimated. For the simulations shown here, $D_s = \log(200)/\log 2^{14} = 0.55$ so that with $C_1 = 0.2$, for all α, $q_s > 2.8$.

Before comparing this formula with the simulations, there is one last practical point we should mention. Numerically, it very advantageous to use transform-based convolution routines and these are periodic. In all our simulations, we therefore used periodic convolutions. Since the noise $\gamma(x)$ is statistically invariant under translations along the x-axis, this will not break the translational invariance, however it does mean that the left half of the simulation is statistically dependent on the right half in a way which is artificially strong (due to the constraint that the resulting $\varepsilon(x)$ is periodic). If absolutely needed, zero padding could be used to avoid the periodicity, or – almost equivalently – only one half of the simulation could be used. One consequence is that the periodic $\varepsilon_{\lambda,\lambda(h)}$ is somewhat modified with respect to its nonperiodic value. Note that due to numerical issues the Fourier filter corresponding to the convolution with $|\underline{x}|^{-D/\alpha}$ is not exactly $|\underline{k}|^{-D/\alpha'}$ (where α' is the auxiliary variable, $1/\alpha'+1/\alpha=1$), so that the inverse transform of $|\underline{k}|^{-D/\alpha'}$ is not strictly positive implying not strictly extremal noises so that convolutions starting in real space should be used (rather than simply taking the inverse transform of pure power law filtered extremal Levy noises).

We can now compare the predictions of Eq. (14) with the simulations shown in Part I Fig. 5. We see that as expected from Eq. (14) that the moments are a little below the theoretical $\lambda^{K(q)}$ values. Also, we see that with the corrections discussed below, that at least for the lower order moments that the moments are nearly perfect if we take $\lambda \to \lambda/2$ (as suggested by the periodicity constraint).

3. The two-point statistics

Following the development for the continuous in scale case, we have the finite difference estimate of S_f

$$S_f(\Delta x) = \sum_{-\lambda \leq \text{odd } i \leq \lambda} (g(i-\Delta x)+g(i))^\alpha \tag{15}$$

(the subscript "f" is to distinguish it from the spatially continuous S; the sum is over odd indices). There are four boundaries which give a large contribution: at $i=\pm 1$, $i=\Delta x+1$, $i=\Delta x-1$, we will ignore the smaller contributions from $i=\pm\lambda$ so that

$$S_f(\Delta x) \approx \frac{1}{2}S(\Delta x) + b_1 + b_2 + \cdots \tag{16}$$

(the factor 1/2 is from the $1/\Delta X$ factor, $\Delta X=2$, see Eq. (7)). b_1, b_2 are the first and second order boundary terms

$$b_1 = \frac{1}{2}[g(-\Delta x-1)+g(-1)]^\alpha + \frac{1}{2}[g(-\Delta x+1)+g(1)]^\alpha + \frac{1}{2}[g(1)+g(\Delta x-1)]^\alpha + \frac{1}{2}[g(1)+g(\Delta x+1)]^\alpha \tag{17}$$

$$b_2 = \frac{1}{6}\frac{\partial[g(x-\Delta x)+g(x)]^\alpha}{\partial x}\bigg|_{x=-1} - \frac{1}{6}\frac{\partial[g(x-\Delta x)+g(x)]^\alpha}{\partial x}\bigg|_{x=1} + \frac{1}{6}\frac{\partial[g(x-\Delta x)+g(x)]^\alpha}{\partial x}\bigg|_{x=\Delta x-1} - \frac{1}{6}\frac{\partial[g(x-\Delta x)+g(x)]^\alpha}{\partial x}\bigg|_{x=\Delta x+1} \tag{18}$$

In the case where g is even, we obtain

$$b_1 = [g(1)+g(\Delta x-1)]^\alpha + [g(1)+g(\Delta x+1)]^\alpha \tag{19}$$

We now use

$$[g(1\pm\Delta x)+g(1)]^\alpha \approx g(1)^\alpha + \alpha g(1)^{\alpha-1}g(\Delta x) + \cdots \tag{20}$$

valid for large Δx (to this order, use $g(1\pm\Delta x)\approx g(\Delta x)$). Using the truncated power law for g (Part I, Eq. (20)), we obtain

Please cite this article as: Lovejoy, S., Schertzer, D., On the simulation of continuous in scale universal multifractals, Part II: Space–time processes and finite size corrections. Computers and Geosciences (2010), doi:10.1016/j.cageo.2010.07.001

(with grid spacing $\Delta X=2$)

$$b_1 = 2(1+\alpha\Delta x^{-1/\alpha}+O(\Delta x^{-2/\alpha})) \quad (21)$$

For the b_2 term involving the first order derivative, we obtain

$$b_2 = -\frac{2\alpha}{3}g'(1)(g(1)^{\alpha-1}+(\alpha-1)g(\Delta x)g(1)^{\alpha-2}) \quad (22)$$

$$b_2 = \frac{2}{3}(1+(\alpha-1)\Delta x^{-1/\alpha}+\cdots) \quad (23)$$

Putting all this together, we obtain

$$S_f(\Delta x) \approx \frac{1}{2}S(\Delta x)+\left(2+\frac{2}{3}+\cdots..\right)+\left(2\alpha+\frac{2\alpha-2}{3}+\cdots\right)\Delta x^{-1/\alpha}+O(\Delta x^{-2/\alpha}) \quad (24)$$

If we now use Part I Eq. (43) for $S(\Delta x)$ (with $N_D=2$ in the place of N_D), we see that aside from unimportant constants and the leading log terms, we have the leading order $\Delta x^{-1/\alpha}$ correction

$$\left(-2\alpha^2+2\alpha+\frac{2\alpha-2}{3}+\cdots\right)\Delta x^{-1/\alpha} \quad (25)$$

we see that the effect of discretization is to somewhat decrease the magnitude of the correction. However for $\alpha=2$ the prefactor is $\approx -10/3$ which is still large (to this order, for $\alpha=1$ it is 0).

Combining the above results with those of Appendix A for the more general g, we obtain the following coefficient of the $\Delta x^{-1/\alpha}$ term

$$2\alpha\left(\int_1^\infty (g(x)^{\alpha-1}-x^{-1+1/\alpha})\,dx-\alpha\right) \quad -2\alpha g(1)^{\alpha-1}-\frac{2}{3}\alpha(\alpha-1)g(1)^{\alpha-2}g'(1)+\cdots \quad (26)$$

4. Removing the $\Delta x^{-D/\alpha}$ term

4.1. A general method of removing the $\Delta x^{-D/\alpha}$ term

We have argued that the presence of the slowly decreasing $\Delta x^{-D/\alpha}$ term is responsible for significant deviations from pure scaling of the two-point statistics, and that the spatial discretization does not change the problem much. In this section we propose various small x modifications to the function $g(x)$ that can eliminate the term.

In Appendix B we show that the $\Delta x^{-D/\alpha}$ behaviour comes from a specific term denoted $S^{(1,1)}$ (Eq. (41)). Considering again the $D=1$ case, for the spatially discrete process, the corresponding term is

$$S_f^{(1,1)} = 2\alpha g(\Delta x)\sum_{1\le i<\Delta x/2,i,odd} g(x)^{\alpha-1} \quad (27)$$

with straightforward extensions to dimensions higher than 1. The factor of 2 between the above and the continuous formula is because we have used $\Delta X=2$. Since $g(x)\approx|x|^{-1/\alpha}$ we must apply the Euler–Maclauren formula to the function $|x|^{1/\alpha-1}$ which yields

$$\sum_{1\le i<\Delta x/2,i,odd} g(i)^{\alpha-1} = \sum_{1\le i<\Delta x/2,i,odd} (|i|^{-1/\alpha})^{\alpha-1} = A+\Delta x^{1/\alpha} \times(B+C\Delta x^{-1}+O(\Delta x^{-2}))\approx A+B\Delta x^{1/\alpha} \quad (28)$$

where A, B are the constants. The theoretical evaluation of the constant A is complicated (it comes from the boundary terms at $x=1$) and $B=\alpha 2^{-1-1/\alpha}$ comes from the integral term, C and higher order Δx^{-1} terms from the boundary terms at $x=\Delta x/2$. Since $g(\Delta x)\approx\Delta x^{-1/\alpha}$ we see that $2\alpha A$ is the desired $\Delta x^{-1/\alpha}$ coefficient. The values of A and B can be directly numerically obtained as described Appendix C.

To eliminate the $\Delta x^{-1/\alpha}$ terms, it now suffices to choose a function g that deviates for small x from the pure power law form in such a way that the constant A in Eq. (28) vanishes. This can be achieved by choosing g of the form

$$g(x) = (1+af(x))^{1/\alpha-1}|x|^{-1/\alpha} \quad (29)$$

where $f(x)$ is a function that falls off rapidly with x (the exact form is not important; for the one-point statistics use of Eq. (29) will add a small constant and small λ dependent terms). If we use Eq. (29) for $g(x)$, we find by summing over the grid

$$\sum_{1\le i<\Delta x/2,i,odd} g(x)^{\alpha-1} \approx (A+B\Delta x^{1/\alpha}+aG) \quad (30)$$

where

$$G \approx \sum_{1\le i<\Delta x/2,i,odd} f(x)|x|^{1/\alpha-1} \quad (31)$$

where we have assumed that $f(x)$ has a rapid enough fall-off, so that the sum in Eq. (31) is nearly independent of the upper limit $\Delta x/2$ (so that G is a constant). For the constant terms in Eq. (30) to disappear, it suffices to choose $a=-A/G$. The only constraint is that the resulting g must be strictly positive so that $af(x)>-1$ for all x. This method has the advantage that the coefficients A, G can be estimated directly numerically, that it readily generalizes to higher dimensions (see Section 4.3) and (as discussed elsewhere) to anisotropic scaling systems (see for example the simulations on http://www.physics.mcgill.ca/~gang/multifrac/index.htm). In the simulations shown here, "$\Delta x^{-1/\alpha}$ corrected" simulations used the exponential choice $f(x)=e^{-|x|/3}$. Numerical investigation shows that the coefficient a is indeed small and as expected is not sensitive to $f(x)$. Indeed, for $\alpha>1$ that even the power law $f(x)=|x|^{-\alpha}$ works and gives nearly the same estimate of the parameter a (ranging from 0 to ≈ 0.4 as α varies from 1 to 2).

In Part I, we gave extensive analyses of the improvements introduced by this correction method, including the conclusion that at least for $\alpha>1$, that the method leads to significant improvements in the statistics, we return to this question in the next two subsections.

4.2. A semi-empirical Δx^{-1} correction method

This paper has primarily been motivated by the desire to improve simulations of universal multifractals for $\alpha>1$, since this apparently corresponds to most of the empirically studied geofields to date. We traced the main difficulty to the $\Delta x^{-D/\alpha}$ terms which in 1-D, for $\alpha>1$ were the leading order corrections. We see however that when $\alpha<1$ (or indeed, $D=2$ or greater) that this correction will fall-off faster than Δx^{-1}. Although in the symmetric causal case the Δx^{-1} terms are zero by symmetry, in the general asymmetric (e.g. causal and/or anisotropic) case there will be potentially important Δx^{-1} terms. This would necessitate correcting for the Δx^{-1} terms. Alternatively, since we saw in Part I, Figs. 3, 5, 6 that numerically correcting for the $\Delta x^{-1/\alpha}$ term lead to large improvements in the simulations for $\alpha=2$, that as expected, the benefit decreased with decreasing α, becoming negligible for $\alpha<1$. In reality as α decreases, terms of many orders will contribute to the small Δx corrections and it is therefore of interest to develop another method of removing them so that $S_f(\Delta x)$ is closer to the theoretically desired pure log behaviour.

One way explored here (see also Appendix D), is to perturb the pure power law g by a small power law correction

$$g(x) = \begin{cases} |x|^{-1/\alpha}(1+\delta|x|^{-\xi}); & |x|\ge 1 \\ 0; & |x|<1 \end{cases} \quad (32)$$

where δ is a small parameter and ξ is an exponent to be determined. By substitution into the formula for $S_f(\Delta x)$, it can be seen that

$$S_f(\Delta x) = S_0(\Delta x)+\delta S_1(\Delta x)+O(\delta^2) \quad (33)$$

Please cite this article as: Lovejoy, S., Schertzer, D., On the simulation of continuous in scale universal multifractals, Part II: Space–time processes and finite size corrections. Computers and Geosciences (2010), doi:10.1016/j.cageo.2010.07.001

where S_0 is the unperturbed $S_f(\Delta x)$ and the first order correction is of the form

$$S_1(\Delta x) = A_{10} + A_{1,-\xi}\Delta x^{-\xi} + A_{1,-\xi-1/\alpha}\Delta x^{-\xi-1/\alpha} + A_{1,-1}\Delta x^{-1} + O(\Delta x^{-\xi-2/\alpha}) + O(\Delta x^{-2}) \quad (34)$$

We therefore see that taking $\xi \approx 1$ leads to

$$S_1(\Delta x) \approx A_{1,0} + A_{1,-1}\Delta x^{-1} \quad (35)$$

(since for any ξ there are always Δx^{-1} terms, there is no benefit to taking $\xi < 1$).

Since the constant term is unimportant, we can use this to improve the simulations by removing the best fit linear function of Δx^{-1}. To implement this numerically, we determine the best fit linear regression of Δx^{-1} to both $S_f(\Delta x)+(2^\alpha-2)\log\Delta x$ (i.e. the deviation from the desired behaviour), as well as to the numerically determined $S_1(\Delta x)$

$$S_0(\Delta x)+(2^\alpha-2)\log\Delta x \approx A_{0,0} + A_{0,-1}\Delta x^{-1} \quad (36)$$

The ratio of the coefficients of the Δx^{-1} terms then determines δ

$$\delta = -A_{0,-1}/A_{1,-1} \quad (37)$$

The regressions to determine $A_{0,0}$, $A_{0,-1}$ were done for Δx up to 20 (the region where these corrections were strongest). The results for the spectra and moments were shown in Part I Figs. 3, 5, 6, respectively. We see that even for the $\alpha=0.8$ case there is some improvement while for $\alpha=0.4$, there is virtually no change. However, for $\alpha > 1$, the corrections were almost as successful as the more theoretically justified removal of the $\Delta x^{-1/\alpha}$ terms as discussed in Section 4.1. Close examination of both the spectra and scale by scale $K(q)$ estimates (Part I, Figs. 3 and 6a) shows that the correction is slightly too strong for the $\alpha=2$ case, that it makes little difference for the $\alpha=0.4$ and 1.6 cases (Part I Figs. 3 and 6b), but is a slight improvement for the $\alpha=0.8$, 1.2, cases (Part I Figs. 3 and 6b). In the $\alpha=1.6$ case, the over-correction in the spectrum for the Δx^{-1} term is apparently about the same magnitude as the under correction in the $\Delta x^{-1/\alpha}$ method caused by the remaining higher order terms.

4.3. Causal and acausal simulations

Up until now, we have made little reference to the problem of space–time simulations, noting mostly that to respect causality, the cascade $\varepsilon_\lambda(\underline{x}, t)$ at time t must be statistically independent of $\varepsilon_\lambda(\underline{x}, t')$ for all $t' > t$ so that the future does not influence the present or past (Part I, Section 3.2.1, see also Part I, 3.3). In Section 2.1 above, it was mentioned that the way to ensure this was to include a Heaviside function $\Theta(t)$ so that for example an acausal $g(\underline{x}, t)$ is transformed into a causal $g_c(\underline{x}, t)=\Theta(t)\, g(\underline{x}, t)$. We also noted that if the acausal g is symmetric so that $g(\underline{x}, t)=g(\underline{x}, -t)$ then the causal normalization constant was simply related to the acausal constant via: $N_{Df,c}=N_{D,f}/2$ (Section 2.2). Aside from this straightforward normalization issue, the correction method—and correction constant a in Eq. (29) are unchanged so that there are very few changes in the numerical implementation; see Appendix C for the simple Mathematica code. In this subsection we proceed to evaluate and intercompare the statistical accuracy of the causal and acausal simulations, as well as the effect of passing from 1-D to 2-D. Since the $\Delta x^{-D/\alpha}$ correction method is simple to implement, works reasonably well and is mathematically well grounded, we do not consider the Δx^{-1} method further. Also, to evaluate the simulations, we only consider the (compensated) spectra i.e. the $q=2$ statistics rather than statistics of all orders. This is sufficient since we find: (a) that the statistics are more accurate for the causal case than for the acausal case, (b) as expected when going from $D=1$ to 2 the convergence is improved, (c) we only consider the case $\alpha=2$ since the corresponding corrections are the largest.

Consider first the causal 1-D simulations. Fig. 1a shows that even without any corrections (blue, 2nd from top) that the causal simulations have significantly smaller deviations from pure power law behaviour than the uncorrected acausal simulations (cyan); indeed they are even comparable to the corrected acausal spectra. With the $\Delta x^{-D/\alpha}$ corrections (green, top) we see that the causal spectrum is nearly perfect. In comparison, the corrected acausal curve (pink, reproduced from Part I, Fig. 3a) has significantly larger deviations.

Turning our attention to simulations in 2-D, we recall the examples of isotropic acausal realizations of the process in Part I, Figs. 1 and 2b. As discussed in Part I, we expect the corrections to

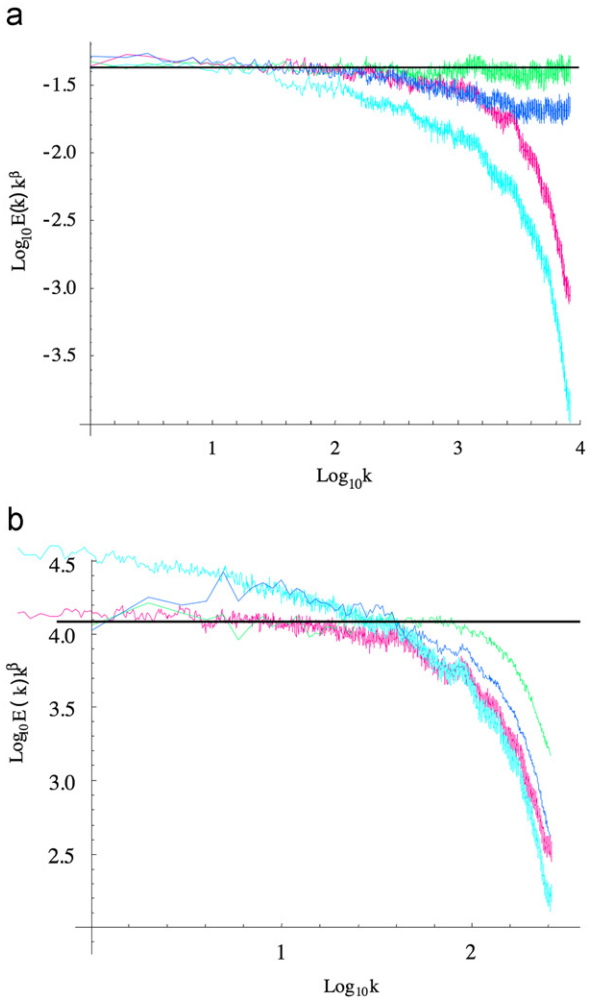

Fig. 1. (a) Compensated spectra for the $D=1$ causal and acausal cases for $\alpha=2$, $C_1=0.2$ averaged over 200 realizations each 2^{14} long (cf. the comparable figures in Part I) both with and without $\Delta x^{-1/\alpha}$ corrections discussed in text; using code in Appendix C. In top to bottom order, green is the corrected causal spectrum, blue uncorrected causal red corrected acausal and the cyan uncorrected acausal simulations. (b) 1-D/2-D (acausal) comparison for $\alpha=2$, $C_1=0.2$ showing compensated spectra. Pink and cyan are 1-D acausal, compensated spectra (respectively, corrected and uncorrected, 200 realizations 2^{14} points; the curves shown to the lowest wavenumbers). Green and blue curves are, respectively, corrected, and uncorrected 2-D cases, (each 10 realizations, $2^9 \times 2^9$ points). They have been shifted horizontally so that the one and two D highest wavenumbers are the same, and they have been shifted in the vertical so that corresponding low wavenumber parts of spectra roughly overlap (i.e. the corrected with the corrected, and the uncorrected with the uncorrected). Vertical scale is arbitrary. Black line is theoretical pure power law spectrum. (For interpretation of the references to color in this figure legend, the reader is referred to the web version of this article).

Please cite this article as: Lovejoy, S., Schertzer, D., On the simulation of continuous in scale universal multifractals, Part II: Space–time processes and finite size corrections. Computers and Geosciences (2010), doi:10.1016/j.cageo.2010.07.001

be smaller for $D=2$ when compared to $D=1$, Fig. 1b confirms this, indeed, we see that the uncorrected 2-D (isotropic, i.e. angle integrated) spectrum is slightly better than the corrected 1-D spectrum, but in all cases the correction method makes the spectra significantly closer to the theoretical pure power form.

In practical terms, the improved convergence in 2-D may not be quite as beneficial as it appears at first sight. For example, after applying the $\Delta x^{-D/\alpha}$ correction, we may attempt to eliminate the remaining biased small scales by degrading the 1-D resolution by a factor of f_1 and the 2-D resolution by a factor of f_2 (when for $\alpha=2$, $C_1=0.2$, Fig. 1b suggests $f_1 \approx 9$, $f_2 \approx 3$). This implies simulations with an extra f_1 degrees of freedom in 1-D, but an extra f_2^2 degrees of freedom in 2-D. However, the calculation time T (using fast convolution numerics) is roughly $T=AN$ (for $N=\Lambda^D$ degrees of freedom in D dimensions with scale ratio Λ; for example with a 2.5 GHz laptop, the Mathematica code in Appendix C yields the constant $A \approx 1.5 \times 10^{-4}$ s). We thus see that if $f_1 \approx f_2^2$ that the overall calculation time is the same for the same final number of degrees of freedom.

Turning our attention to causal simulations, an example of a realization of a causal process is shown in Fig. 2 where – to emphasize that the simulation is of the temporal evolution of a 1-D series – we have plotted a sequence of spatial sections. Since space and time are no longer symmetric, we evaluated compensated 1-D spectra in the spatial and temporal directions separately; see Fig. 3. We see that the temporal spectra are very close to those of the 1-D causal processes (Fig. 1a)—for both the corrected and uncorrected cases (green, blue, respectively). Similarly, the spectra of the corrected and uncorrected cases in the spatial direction (pink and cyan, respectively) have much larger deviations; very close to the acausal 1-D results (Fig. 1a) and compare with the 2-D acausal spectra (Fig. 1b). We conclude that the correction method works well independently of the dimension of the space and that for the causal extensions that the temporal statistics have significantly smaller deviations. This is presumably because of the sharp discontinuity introduced by the Heaviside function which roughens the simulations along the time axis, this thereby somewhat compensating for the otherwise overly smooth behaviour.

As a final comment, it might be thought that one could use this more accurate causal result to produce improved acausal simulations by taking the product of two statistically independent causal realizations, one with the direction of time reversed (and with the C_1's appropriately reduced). However, numerical experimentation shows that this leads to no improvement whatsoever, so that the $\Delta x^{-D/\alpha}$ method is much better.

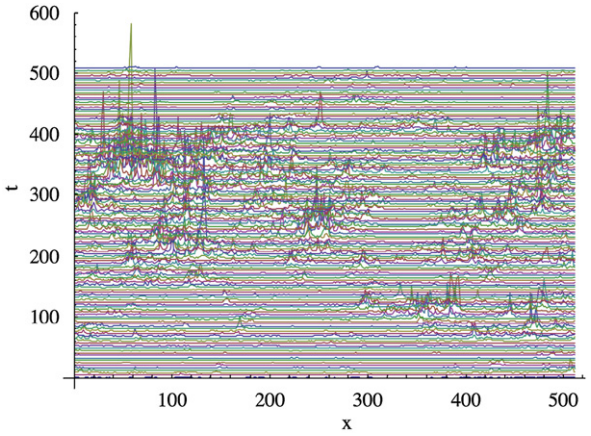

Fig. 2. Evolution of (left right symmetric) 1-D spatial sections, series of a causal simulation with $\alpha=2$, $C_1=0.2$, each second time interval is shown, and is displaced by two units in time axis with respect to previous section.

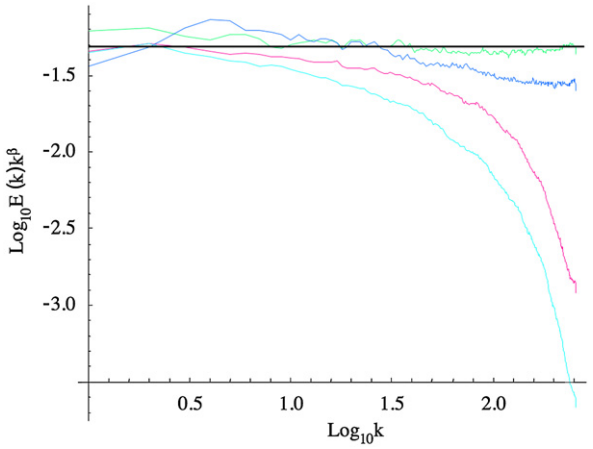

Fig. 3. Compensated spectra for $D=2$ causal simulations for $\alpha=2$, $C_1=0.2$ averaged over 10 realizations each $2^9 \times 2^9$ (cf. Fig. 2) both with and without $\Delta x^{-D/\alpha}$ corrections; using code in Appendix C. In top to bottom order; green is 1-D spectrum of $\Delta x^{-D/\alpha}$ corrected simulations in t direction; blue corresponding spectra of uncorrected simulations; red 1-D spectrum of $\Delta x^{-D/\alpha}$ corrected simulations in x direction and cyan corresponding 1-D spectrum of uncorrected simulations (For interpretation of the references to color in this figure legend, the reader is referred to the web version of this article).

5. Conclusions

When nonlinear dynamical systems respect a (possibly anisotropic) scale invariant symmetry, it is common to observe multifractal statistics with corresponding underlying (turbulent-like) fluxes following cascade processes. This has just recently been strikingly demonstrated both in the case of conventional global weather models – which display nearly perfect cascade structures down to their inner dissipation scales (Stolle et al., 2009) – and in the case of short and long wave satellite measured radiance fields (Lovejoy et al., 2009; see Lovejoy and Schertzer, 2010 for a review). Similarly, the key solid earth field – the topography – also accurately shows cascade behaviour down to at least 40 m (Gagnon et al., 2006). Due to the importance of these fields in many areas of geoscience, techniques to produce realistic (continuous in scale) cascade processes are widely needed. It is therefore at first sight paradoxical that the relatively few attempts at direct stochastic simulations of cascade processes have almost invariably been discrete in scale. This implies that power law scaling only holds for scale ratios which are integer powers of integers so that for almost all scale ratios there are strong statistical deviations; these turn out to be associated with the appearance of unsightly artifacts on random realizations. Although a visually and theoretically attractive alternative continuous in scale cascade process with the desired pure power law scaling was proposed over twenty years ago, their internal structures had strong "finite size effects" so that convergence to the theoretical behaviour was often painfully slow.

In Part I of this two part series, we showed that for spatially isotropic processes (leading to self-similar cascades, to self-similar multifractals), that the leading contribution to these corrections was a $\exp(-\Delta x^{-D/\alpha})$ term multiplying the pure power law autocorrelation function. In this second part, we examined the consequences of spatially discretising a continuous in scale cascade process—finding that it added smaller terms of essentially the same type so that the basic problem was unchanged. Our next task was therefore to consider various methods of reducing the bias, the preferred method involving removal of the $\Delta x^{-D/\alpha}$ term altogether. Although there are still residual biases due to the even higher order terms, the method makes a significant improvement for the empirically significant large α

Please cite this article as: Lovejoy, S., Schertzer, D., On the simulation of continuous in scale universal multifractals, Part II: Space–time processes and finite size corrections. Computers and Geosciences (2010), doi:10.1016/j.cageo.2010.07.001

part of the range. We also considered a semi-empirical correction method that was somewhat better than the $\Delta x^{-1/\alpha}$ method for $\alpha<1$ as well as a less successful complex singularity method (Appendix D).

Although we mostly concentrated on the acausal 1-D case, we showed how to generalize to the higher dimensional isotropic (self-similar) cascades as well as to the causal simulations needed for simulating space–time processes; all that was required was the multiplication by a Heaviside function and a small change in the normalization coefficients. We found that the corrections for the temporal statistics in 1-D time or in space–time processes were significantly less important than for the corresponding spatial statistics. This was probably because the discontinuities introduced by the Heaviside function "roughened" the process, partially compensating for the smoothing associated with the finite size corrections. While we did not explore further generalizations, all of these results (including the correction method) can be generalized to anisotropic scaling, essentially by replacing the fractional integrations defined by convolutions with powers of the usual vector norm by the corresponding fractional integrations defined by convolutions with powers of anisotropic scale functions. Investigating these anisotropic simulations will be the subject of a future publication.

Acknowledgements

One of the authors (SL) would like to thank the Laboratoire de Modelisation en Méchanique for hosting a sabbatical (2002-2003) where much of this work was done. This work was done for scientific purposes only, it was unfunded.

Appendix A. The $\Delta x^{-1/\alpha}$ term for general g in 1-D

We have seen that $S(\Delta x)$ can be expressed as the sum of an (unimportant) constant, a logarithmic term followed by a $\Delta x^{-1/\alpha}$ term which for a pure power law g, can be fairly large. In Section 4, we modified g in order to eliminate this leading correction term, we therefore seek a formula for more general (but still symmetric acausal, even) g (c.f. Part I, Eqs. (36) and (37)) only constrained such that $g(x)\approx|x|^{-1/\alpha}$ for large enough $|x|$.

The first step is rewrite S as

$$S(\Delta x)=2\int_1^{\Delta x/2} g(\Delta x)^\alpha\left[\left(1+\frac{g(x-\Delta x)}{g(\Delta x)}\right)^\alpha+\left(1+\frac{g(x+\Delta x)}{g(x)}\right)^\alpha\right]dx +2\int_{\Delta x/2}^{\lambda} g(x)^\alpha\left(1+\frac{g(x+\Delta x)}{g(x)}\right)^\alpha dx -\int_{\lambda-\Delta x}^{\lambda} g(x)^\alpha\left(1+\frac{g(x+\Delta x)}{g(x)}\right)^\alpha dx \tag{38}$$

and to note that the origin of the $\Delta x^{-1/\alpha}$ term is in the second term of a binomial expansion of the first term on the right $S^{(1)}(\Delta x)$

$$S_{(1)}(\Delta x)=2\alpha\int_1^{\Delta x/2} g(x)^{\alpha-1}(g(\Delta x+x)+g(\Delta x-x))\,dx \tag{39}$$

To estimate this, we can make a Taylor expansion of $g(\Delta x+x)+g(\Delta x-x)$ about the point Δx to obtain

$$S_{(1)}(\Delta x)=4\alpha g(\Delta x)\int_1^{\Delta x/2} g(x)^{\alpha-1}\,dx +2\alpha g^{(2)}(\Delta x)\int_1^{\Delta x/2} x^2 g(x)^{\alpha-1}\,dx+O(g^{(4)}(\Delta x)) \tag{40}$$

where $g^{(n)}$ denotes the nth derivative of g. If g is asymptotically $x^{-1/\alpha}$ (i.e. if $g(x)\approx|x|^{-1/\alpha};\quad|x|\gg1$) then the expansion converges since $x^{2n}g^{(2n)}(x)\approx x^{2n-1+1/\alpha}$, and $g^{(2n)}(\Delta x)\approx\Delta x^{-2n-1/\alpha}$. The result is that the upper bounds of the integrals contributes to (unimportant) constant terms while the lower bounds to terms of order $\Delta x^{-2n-1/\alpha}$.

The contribution to the $\Delta x^{-1/\alpha}$ term is thus from the first term of the Taylor expansion

$$S^{(1,1)}(\Delta x)=4\alpha g(\Delta x)\int_1^{\Delta x/2} g(x)^{\alpha-1}\,dx \tag{41}$$

since for large Δx, $g(\Delta x)\approx\Delta x^{-1/\alpha}$ this expression can be estimated using the identities

$$S^{(1,1)}(\Delta x)=4\alpha g(\Delta x)\int_1^{\Delta x/2}(g(x)^{\alpha-1}-x^{-1+1/\alpha})\,dx+4\alpha^2 g(\Delta x)\left(\left(\frac{\Delta x}{2}\right)^{1/\alpha}-1\right) \tag{42}$$

and

$$\int_1^{\Delta x/2}(g(x)^{\alpha-1}-x^{-1+1/\alpha})\,dx =\int_1^{\infty}(g(x)^{\alpha-1}-x^{-1+1/\alpha})\,dx-\int_{\Delta x/2}^{\infty}(g(x)^{\alpha-1}-x^{-1+1/\alpha})\,dx \tag{43}$$

The first term on the right is a constant, the second of order $\Delta x^{-1+1/\alpha}$ so that obtain

$$S^{(1,1)}(\Delta x)\approx 4\alpha g(\Delta x)\int_1^{\infty}(g(x)^{\alpha-1}-x^{-1+1/\alpha})dx-4\alpha^2 g(\Delta x)+B \tag{44}$$

where B is an unimportant constant. Finally, for large Δx, $g(\Delta x)\approx|\Delta x|^{-1/\alpha}$ so that

$$S^{(1,1)}\approx C_{-1/\alpha}\Delta x^{-1/\alpha}+B;$$
$$C_{-1/\alpha}=2\alpha\left(\int_1^{\infty}(g(x)^{\alpha-1}-x^{-1+1/\alpha})\,dx-\alpha\right) \tag{45}$$

We can see that for the pure truncated power law case, $g(x)=|x|^{-1/\alpha}$, the integrand vanishes and we have

$$C_{-1/\alpha}=-2\alpha^2 \tag{46}$$

which is the result we obtained earlier (Part I, Eq. (43) with $D=1$).

Appendix B. 2D and higher

B.1. $D=2$

In Part I, Section 3, we explicitly treated the $D=1$ case but anticipated the higher dimensional results by writing key equations with D as a parameter. Consideration of the $D=2$ case justifies this further and demonstrates how to generalize this to the treatment of higher dimensional isotropic systems. First, for a D-dimensional vector, in standard vector notation the unnormalized log autocorrelation function is

$$S(\underline{\Delta x})=\int_{1<|\underline{x}|<\lambda}\left(1+\frac{g(\underline{x}-\underline{\Delta x})}{g(\underline{x})}\right)^\alpha g(\underline{x})^\alpha d^D\underline{x} \tag{47}$$

As discussed earlier, since are considering isotropic multifractals, $g(\underline{x})=g(|\underline{x}|)$ so that without loss of generality, we can take $\underline{\Delta x}$ parallel to the x-axis and we can introduce the same basic transformations of variables as in the 1-D case

$$r=\frac{|\underline{x}|}{|\underline{x}-\underline{\Delta x}|} \tag{48}$$

From geometrical considerations in $D=2$, we find that the distance ratio r is constant on circles radius R centred at $(-Rr,0)$ where

$$R=\frac{r\Delta x}{1-r^2} \tag{49}$$

Please cite this article as: Lovejoy, S., Schertzer, D., On the simulation of continuous in scale universal multifractals, Part II: Space–time processes and finite size corrections. Computers and Geosciences (2010), doi:10.1016/j.cageo.2010.07.001

(in higher dimensions, r is constant on (hyper) spheres with the same R and centre). Rather than using the usual planar polar coordinates centred at the origin $(|\underline{x}|,\varphi)$ we can therefore specify a point in space by polar coordinates centred at $(-Rr, 0)$ with angle from the x-axis θ and with the distance from this centre parametrized by r—which from Eq. (49) we see is a nonlinear function of the radius R. In $D=2$, we find the following relation between the coordinates

$$x = |\underline{x}|\cos\varphi = R(\cos\theta - r)$$
$$y = |\underline{x}|\sin\varphi = R\sin\theta \tag{50}$$

The region $r<1$ corresponds to the half plane $x<\Delta x/2$ whereas the region $r>1$ corresponds to the half plane $x>\Delta x/2$; extensions to higher dimensional spaces are straightforward.

Now consider expressing the integral Eq. (47) in terms of the new coordinates. Fig. 4 shows a schematic with the region of integration shown between the large radius λ black circle and the two small black unit circles (due to the truncation of g). The large and small blue and pink circles are respectively the largest and smallest r=constant circles which can be inscribed within the region of integration.

To evaluate the integrals, we now take

$$g(\underline{x}) = |\underline{x}|^{-D/\alpha}; |\underline{x}|>1; 0; |\underline{x}|<1; \qquad D=2 \tag{51}$$

and notice from Eq. (47) that the important measure density is $g(\underline{x})^{\alpha}d^D\underline{x}$. From the transformation of variables (Eq. (50)) and using $g^{\alpha}\approx|\underline{x}|^{-D}$ we find for $D=2$

$$g(\underline{x})^{\alpha}d^2\underline{x} = \frac{dx\,dy}{(x^2+y^2)} = d\log|\underline{x}|d\varphi = \frac{dr\,d\theta}{r(1-r^2)} \tag{52}$$

Now consider just the integration over r values corresponding to circles between in the inner and outer blue and inner and outer pink circles in the figure (indicated in the figure $S_<$, $S_>$, respectively); for these the θ integral just gives 2π and we obtain $S_{circles}(\Delta x)$

$$S_{circles}(\Delta x)\approx S_< + S_> = 2\pi\int_{1/(1+\Delta x)}^{1/(1+\Delta x/\lambda)}(1+r^{D/\alpha})^{\alpha}\frac{dr}{r(1-r^2)} + 2\pi\int_{(\Delta x-1)}^{1/(1-\Delta x/\lambda)}(1+r^{D/\alpha})^{\alpha}\frac{dr}{r(1-r^2)} \tag{53}$$

with $D=2$. The difference between $S_{circles}(\Delta x)$ and $S(\Delta x)$ due to the mismatch in the upper limits of integration is $O(\Delta x/\lambda)$ and that due to mismatches in the lower limits of integration is $O(\Delta x^{-2})$, therefore for our purposes, $S_{circles}(\Delta x)\approx S(\Delta x)$.

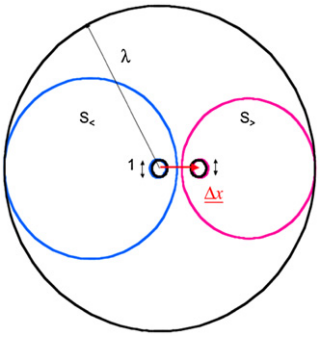

Fig. 4. Schematic showing various regions of integration with large, thick black circle at radius l; small black circles have radius 1 and are around the origin and the point (Dx,0); which cutoff off singularities (to avoid clutter, axes have not been shown: horizontal is x direction, vertical, y direction). $\underline{Dx}$ is in x direction as shown and satisfies $1<Dx<l$. $S_<$ is the set bounded between blue lines with $r=1/(1+\Delta x)$ (small blue circle) and $r=(1+\Delta x/\lambda)$ (large blue circle). $S_>$ is the set bounded between pink circles with $r=(\Delta x-1)$ (small pink circle), and $r=1/(1-\Delta x/\lambda)$ (large pink circle) (For interpretation of the references to color in this figure legend, the reader is referred to the web version of this article).

Finally, we note that the integrand is invariant under the transformation $r\to 1/r$, and we find that – again to within errors of the order Δx^{-2} and $(\Delta x/\lambda)^{-2}$ – the two integrals in Eq. (53) are in fact equal so that we finally obtain

$$S(\Delta x) = 2N_D\int_{\Delta x^{-1}}^{1/(1+\Delta x/\lambda)}(1+r^{D/\alpha})^{\alpha}\frac{dr}{r(1-r^2)} + O\left(\frac{\Delta x}{\lambda}\right) + O(\Delta x^{-2});$$
$$D=2; \quad N_D = 2\pi \tag{54}$$

where the normalization $N_D=2\pi$ in $D=2$ dimensions. We see that this is identical to the $D=1$ result, Part I Eq. (41) so we can immediately conclude that the leading correction to the logarithmic behaviour is

$$-\frac{2\alpha^2}{D}\Delta x^{-D/\alpha} \tag{55}$$

and that the overall correction to the correlation function is the factor

$$\exp\left(-\frac{2\alpha^2 C_1}{D(\alpha-1)}\Delta x^{-D/\alpha}\right) \tag{56}$$

valid for $D=1, 2$; below we argue that it is also valid for $D=3$ and higher dimensions.

B.2. Isotropic $D=3$ (and higher) cases

From the 2-D isotropic analysis, it can be seen that in $D=3$ (and higher) the same approach based on the distance ratio transformation of variables can be used (Eq. (49)). In this case, the (hyper) surfaces of constant distance ratio r are (hyper) spheres, and the only difference is the form of the D-dimensional measure density $d^D\underline{x}/|\underline{x}|^D = d\log|\underline{x}|\,d\Omega_D$; we saw that in 2D this was particularly simple. Direct calculation of the basic logarithmic integration element $d\log|\underline{x}|\,d\Omega_D$ in 3-D yields (cf. Eq. (52))

$$d\log|\underline{x}|\,d\Omega_D = \frac{dr}{r(1-r^2)}\frac{\sin\theta\,d\theta\,d\phi}{\sqrt{1+r^2-2r\sin\theta}} \tag{57}$$

where θ, ϕ are the spherical polar angles of the r=constant spheres with respect to the centres of the spheres at $(0,0,-Rr)$; we have taken the $\underline{\Delta x}$ vector parallel to the z-axis. Comparing this to the 2-D result (Eq. (52)) we see that the basic singularity with respect to r is the same, but that there is an extra term that depends on θ. However, integrating over all the θ, ϕ angles we find

$$\int_0^{\pi}\int_0^{2\pi}\frac{\sin\theta\,d\theta\,d\phi}{\sqrt{1+r^2-2r\sin\theta}} = 4\pi = \Omega_D = N_D; \quad D=3 \tag{58}$$

(independent of r) so that the 3D isotropic results are identical to the 2-D isotropic results. The fundamental reason is that the r=constant (hyper) surfaces are (hyper) spheres displaced form the origin by $-Rr$, the total angle subtended is the same. We can see that in higher D, the same structure will remain: if we integrate over the angles in the r=constant (hyper) spheres, we will obtain: $\int_{\Omega_D} d^D\underline{x}/|\underline{x}|^D = dr/r(1-r^2)\Omega_D$ so that using $N_D=\Omega_D$, we recover Part I, Eq. (23) and find that the SCF (which depends on $N_D^{-1}S$ Part I, Eq. (27)) is the same.

Appendix C. Mathematica code

The Mathematica code reproduced in Fig. 5 implements the $\Delta x^{-D/\alpha}$ correction scheme described in Section 4.1 in both 1D and 2D for causal and acausal processes. *Levy* generates random extremal Levy variables attention is paid to avoiding underflows

```
nuni = UniformDistribution[{-Pi/2, Pi/2}]
```

$$\texttt{UniformDistribution}\left[\left\{-\frac{\pi}{2},\frac{\pi}{2}\right\}\right]$$

```
this gives a uniform between - Pi/2 and + Pi/2
```

```
ndist[lam_] := ExponentialDistribution[lam]
RanE[lam_] := Random[ndist[lam]]
Levy[α_] := Module[{ϕ, ϕ0}, {ϕ = Random[nuni], ϕ0 = -(Pi/2) (1 - Abs[1-α])/α
```

```
This gives unit extremal Levy variables index α
```

```
Fracε[scal_, α_] := Module[{A, a, λ}, {λ = Min[Dimensions[scal]], rat =2., αp
      lcut = λ/2., lcut2 = lcut/rat,
      exλ = Chop[E^(-(scal/lcut)^4 /. x_ /; x < -200. -> -200.)],
      exλ2 = Chop[E^(-(scal/lcut2)^4 /. x_ /; x < -200. -> -200.)],
      sing = (scal)^-(1/αp), singsmooth = Chop[ sing  exλ],
      t1 = Total[Flatten[singsmooth]],
      singsmooth = Chop[ sing  exλ2 ],
      t2 = Total[Flatten[singsmooth]],
      A = (rat^-(1./α) t1 - t2)/(rat^-(1./α) - 1),
      ff = Chop[E^(-(scal/3.) /. x_ /; x < -200. -> -200.)],
      singsmooth = Chop[sing   ff],
      G = Total[Flatten[singsmooth]],
      a = -A/G, sing =  Chop[( sing  (1 + a  ff))]^(1/(α - 1.))}; sing]
```

```
this calculates the corrected singularity
```

```
eps1D[λ_, α_, C1_, switch_] := Module[{ff, xx}, {NDf = If[switch == 0, 1, 0.5
      ggen1α = ListConvolve[ggen1, Heavi  sing, 1], ggen1α = ggen1α /.x_ /;x
```

```
1 D  causal (switch not zero) and acausal (switch = 0)
```

```
eps2D[λt_, λy_, α_, C1_, switch_] := Module[{ff, tt}, {NDf = Pi/2  If[switch
```

```
2 D  causal (switch not zero) and acausal (switch = 0)
```

Fig. 5. Code for producing causal and acausal isotropic 1-D and 2-D universal multifractals corrected for $\Delta x^{-1/\alpha}$ terms. If switch=0, the simulation is acausal, otherwise it is causal. The code Chop[E−^(-(scal/lcut)^4 /. x_ /; x < −200. − > −200.)] indicates thresholded exponentiation (with small remainders chopped to zero), necessary to avoid underflows. Extensions to isotropic 3-D simulations are straightforward.

when exponentiating (important for α). The basic functions *epsa, epsc* generate the corrected multifractal acausal, causal simulations; λ is the length of the resulting vector, α, C_1 are the basic parameters. Note that as mentioned in the text, the built-in function *Convolve* performs a periodic convolution (no zero padding was used).

The routine *Fracε* evaluates the sums in Eqs. (30) and (31) by using the scaling property of the summands. The basic idea is to replace the sum with upper cutoff $\Delta x/2$ (Eqs. (30) and (31)) by an infinite sum but with a smooth cutoff function $h(x)$

$$t_1 = \sum_{i=1}^{\infty} g(i)^{\alpha-1} h(2i/\Delta x)$$
$$t_2 = \sum_{i=1}^{\infty} g(i)^{\alpha-1} h(2i/(r_t \Delta x)) \quad (59)$$

Then using the scaling property of g, we obtain

$$A \approx \frac{t_1 r_t^{-1/\alpha} - t_2}{r_t^{-1/\alpha} - 1} \quad (60)$$

Here we take $h(x) = \exp(x^{-4})$, $r_t = 2$ (in the code, the symbol "rat"). This has the advantage of being numerically robust (especially when generalized to higher dimensions and strongly anisotropic cascades). A similar technique was used to estimate G in Eq. (31).

Appendix D. Complex singularities

The correction terms to the pure logarithmic behaviour of $S_f(\Delta x)$ are due to summing/integrating singularities which lie on the real axis. It is therefore tempting to explore the consequences

Please cite this article as: Lovejoy, S., Schertzer, D., On the simulation of continuous in scale universal multifractals, Part II: Space–time processes and finite size corrections. Computers and Geosciences (2010), doi:10.1016/j.cageo.2010.07.001

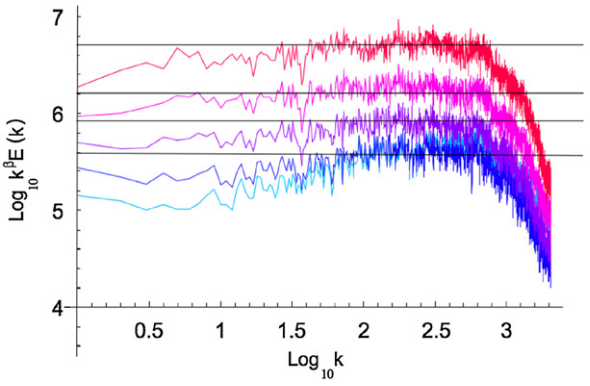

Fig. 6. Compensated spectra for conservative multifractals $\alpha=1.1, 1.3, \ldots, 1.9$ (bottom to top) offset for clarity. Each is average of 20 realizations of 2^{12}. Note that we use the $g(x)$ of the form given in Eq. (63) with $u=\pi/2$, $w=\pi/(2\alpha)$ (this is a convenient, not optimum choice).

of moving the singularities off the real axis, following for example the idea of the "Cauchy" wavelet (Holschneider, 1995). The straightforward application of this idea is to take

$$g(x) = \mathrm{Re}[(1-i|x|)^{-1/\alpha}]; \quad \alpha > 1 \tag{61}$$

the Mathematica code of a 2-D version of this method was given in Schertzer et al. (2002).

More generally, we may consider

$$g(x) = \sec\left(\frac{u}{\alpha}\right)\mathrm{Re}\left[\left(e^{iu}|x|\left(-\frac{se^{i\omega}}{|x|}\right)\right)^{-1/\alpha}\right] \quad \begin{matrix} \frac{\pi}{2} > |u| > 0 \\ \pi > |u+\omega| > \frac{\pi}{2} \end{matrix} \tag{62}$$

where the parameters u, ω, s are constrained so that g is positive for $|x| \geq 1$. It turns out that this is only possible for $\alpha > 1$ so that this "complex singularity" method does not work for $\alpha < 1$ (various extensions for $\alpha < 1$ can be made but they are problematic due to the rapid variation of the exponent $1/\alpha$ which is > 1; these extensions did not lead to large improvements). Note that the normalization in the above has been chosen so that to leading order $g \approx |x|^{-1/\alpha}$

$$g(x) = |x|^{-1/\alpha}\left(1+\frac{\cos(\omega-u/\alpha)}{\alpha\cos(u/\alpha)}\left(\frac{s}{|x|}\right)+O\left(\frac{s}{|x|}\right)^2\right); \quad |x| \geq 1 \tag{63}$$

We see that this correction to the pure power law $|x|^{-1/\alpha}$is of the type discussed in the Appendix D with $\xi=1$, i.e. it leads to Δx^{-1} corrections. In fact, detailed analysis shows that for $S(\Delta x)$ the sum of the $\Delta x^{-1/\alpha}$ and Δx^{-1} terms are

$$\left\{-4\alpha^2+s\left(\frac{\cos(\omega-u/\alpha)}{\cos u/\alpha}\right)\left[4\alpha-8(1+2^{-1/\alpha})\Delta x^{1/\alpha-1}\right]\right\}\Delta x^{-1/\alpha} \tag{64}$$

The problem is that the quantity in the square bracket is only a function of α and changes sign at a fairly small cross-over point Δx_c. For example in the main range of interest $1.5 < \alpha < 2$ we have $10 < \Delta x_c < 3$. From the formula, one can see that the three free "shape" parameters s, ω, u simply modulate this "sliding" term so that there will always be a sizeable combined $\Delta x^{-1/\alpha}$, Δx^{-1} correction. A simplified form of this method was given in (Schertzer et al., 2002)—and as can be seen in Fig. 6 it does improve over the pure truncated singularity results (especially for α near 2). However, the method of Section 4.1 which just removes the $\Delta x^{-1/\alpha}$ term without introducing a new Δx^{-1} term is preferable.

References

Bolgiano, R., 1959. Turbulent spectra in a stably stratified atmosphere. Journal of Geophysical Research 64, 2226–2229.
Charney, J.G., 1971. Geostrophic turbulence. Journal of Atmospheric Science 28, 1087–1091.
Corrsin, S., 1951. On the spectrum of isotropic temperature fluctuations in an isotropic turbulence. Journal of Applied Physics 22, 469–473.
Gagnon, J., Lovejoy, S., Schertzer, D., 2006. Multifractal earth topography. Nonlinear Processes in Geophysics 13, 541–570.
Holschneider, M., 1995. Wavelets: An Analysis Tool. Clarendon Press, Oxford, New York.
Kolmogorov, A.N., 1941. Local structure of turbulence in an incompressible liquid for very large Reynolds numbers. Proceedings of the Academy of Science of the USSR, Geochemistry Section 30, 299–303 (English translation: Proceedings of the Royal Society A434, 9–17, 1991).
Kraichnan, R.H., 1967. Inertial ranges in two-dimensional turbulence. Physics of Fluids 10, 1417–1423.
Lovejoy, S., Schertzer, D., 2007. Scaling and multifractal fields in the solid earth and topography. Nonlinear Processes in Geophysics 14, 1–38.
Lovejoy, S., Schertzer, D., 2010. Towards a new synthesis for atmospheric dynamics: space–time cascades. Atmospheric Research 96, 1–52. doi:10.1016/j.atmosres.2010.1001.1004.
Lovejoy, S., Schertzer, D., Allaire, V., Bourgeois, T., King, S., Pinel, J., Stolle, J., 2009. Atmospheric complexity or scale by scale simplicity? Geophysical Research Letters 36 L01801 Doi:01810.01029/02008GL035863.
Mandelbrot, B.B, 1967. How long is the coastline of Britain? Statistical self-similarity and fractional dimension. Science 155, 636–638.
Obukhov, A., 1949. Structure of the temperature field in a turbulent flow. Izvestia Akademie Nauk, SSSR, Serie Geographia I Geofizica 13, 55–69.
Obukhov, A., 1959. Effect of archimedean forces on the structure of the temperature field in a turbulent flow. Doklady Akademie Nauk SSSR 125, 1246–1249.
Perrin, J., 1913. Les Atomes. NRF-Gallimard, Paris.
Richardson, L.F., 1922. Weather Prediction by Numerical Process, 1965. Cambridge University Press republished by Dover 223 pp.
Richardson, L.F., 1926. Atmospheric diffusion shown on a distance-neighbour graph. Proceedings of the Royal Society A110, 709–737.
Richardson, L.F., 1961. The problem of contiguity: an appendix of statistics of deadly quarrels. General Systems Yearbook 6, 139–187.
Rodriguez-Iturbe, I., Rinaldo, A., 1997. Fractal River Basins. Cambridge University Press, Cambridge 547 pp.
Schertzer, D., Lovejoy, S., 1987. Physical modeling and analysis of rain and clouds by anisotropic scaling of multiplicative processes. Journal of Geophysical Research 92, 9693–9714.
Schertzer, D., Lovejoy, S., Hubert, P., 2002. An introduction to stochastic multifractal fields. In: Liu, A.E.a.W. (Ed.), Mathematical Problems in Environmental Science and Engineering, Series in Contemporary Applied Mathematics, vol. 4. Higher Education Press, Beijing, pp. 106–179.
Schertzer, D., Lovejoy, S., Lavallée, D., 1993. Generic multifractal phase transitions and self-organized criticality. In: Perdang, J.M., Lejeune, A. (Eds.), Cellular Automata: Prospects in Astronomy and Astrophysics. World Scientific, pp. 216–227.
Steinhaus, H., 1954. Length, shape and area. Colloquium Mathematicum III, 1–13.
Stolle, J., Lovejoy, S., Schertzer, D., 2009. The stochastic cascade structure of deterministic numerical models of the atmosphere. Nonlinear Processes in Geophysics 16, 1–15.
Szépfalusy, P., Tél, T., Csordas, A., Kovas, Z., 1987. Phase transitions associated with dynamical properties of chaotic systems. Physical Review A 36, 3525–3538.

Please cite this article as: Lovejoy, S., Schertzer, D., On the simulation of continuous in scale universal multifractals, Part II: Space–time processes and finite size corrections. Computers and Geosciences (2010), doi:10.1016/j.cageo.2010.07.001